Polymer 74 (2015) 205–215

Contents lists available at ScienceDirect

Polymer

journal homepage: www.elsevier.com/locate/polymer

# Control of polymer-packing orientation in thin films through chemical structure of D-A type polymers and its application in efficient photovoltaic devices

Min-Hee Choi, Eui Jin Ko, Yong Woon Han, Eui Jin Lee, Doo Kyung Moon*

*Department of Materials Chemistry and Engineering, Konkuk University, 1 Hwayang-dong, Gwangjin-gu, Seoul 143-701, South Korea*

ARTICLE INFO

*Article history:*
Received 20 April 2015
Received in revised form
30 July 2015
Accepted 3 August 2015
Available online 6 August 2015

*Keywords:*
Orientation
Molecular engineering
D-A type polymer

ABSTRACT

Controlling solid-state order of π-conjugated polymers through macromolecular design is essential for achieving high electronic device performance. Our work investigates the various effects of polymer structure on solid-state packing, especially, regarding polymer-packing orientation (edge-on vs. face-on). Various number of thiophene-containing isoindigo polymers (P4TI, P4TI-3, P4TI-4, P6TI-3 and P6TI-4) are synthesized via Stille coupling reaction. Differences in side chain position and spacer length are attributed to variation in energy levels and polymer backbone curvature. The orientation of the obtained polymers in thin films is confirmed by XRD measurement. Polymers (P4TI, P6TI-4) with shoulder peaks in UV–vis spectra of solution and film exhibit crystalized domains. Planar polymers prefer face-on orientation and provide more efficient organic photovoltaic (OPV) devices. The polymer solar cells are fabricated through a solution process and compared power conversion efficiency (PCE). P6TI-4 shows PCE up to 3.5%, with a short-circuit current density of 7.2 mA/cm$^2$, an open-circuit voltage of 0.70 V, and a fill factor of 66%.



## 1. Introduction

Polymer solar cells (PSCs) have received considerable attention as promising alternatives to inorganic photovoltaic devices in academic research and industrial applications in recent years due to their lightweight, flexible, inexpensive manufacturing and the possibility of large scale production by solution processing [1]. The general architecture of the active layer of PSCs is designed to achieve high efficiency in the bulk heterojunction (BHJ) configuration comprising an electron-donor (conducting polymer) and electron-acceptor (fullerene derivative) combination [2,3]. High-performance BHJ solar cells can be fabricated using a rational design to achieve the optimal configuration of numerous chemical and structural parameters, such as conjugated backbones and side chains [4]. In particular, the donor-acceptor (D-A) concept has been widely applied to the design of the conjugated polymer main chain of PSCs [5]. Using this approach, the frontier molecular orbital energy levels of the target-alternating conjugated copolymer can be obtained with precision through fine-tuning via intramolecular charge transfer (ICT), thus achieving a low band gap. The drawbacks of this approach are that they show dual-band absorption spectra and poor energy harvesting in the range of 400–600 nm, which is the key wavelength of solar radiation that reaches the surface of the Earth.

Isoindigo has two electron-deficient lactam rings with a planar structure and thus exhibits excellent electron-withdrawing ability. Due to this unique advantage, isoindigo has recently garnered attention as an acceptor unit in the synthesis of D–A alternating type low band gap conjugated polymers for solar cells. In 2010, the Reynolds' group performed spectral engineering using the intramolecular donor-acceptor interactions to develop a polymer for full solar spectrum absorption [6] and succeeded in developing oligomer-based organic solar cells using isoindigo as a dye [7]. Although the UV absorption spectrum was extended to 744 nm (band gap: 1.67 eV), the power conversion efficiency (PCE) was still low (1.76%) [8]. Since then, a large number of isoindigo-containing conjugated polymers have been synthesized and utilized for PSCs [9]. The highest PCE ever reported was 7% [10]. Although numerous isoindigo-based donor polymers have demonstrated intense and broad absorption, the organic photovoltaics (OPVs) based on isoindigo-containing conjugated polymers have been reported to

* Corresponding author.
*E-mail address:* dkmoon@konkuk.ac.kr (D.K. Moon).

http://dx.doi.org/10.1016/j.polymer.2015.08.003
0032-3861/

have a low PCE despite the low band gap [11,12]. This is attributable to the fact that intense and broad absorption, which is important for the donor polymer, does not necessarily ensure a high PCE. For efficient transport of the electron/hole generated by solar energy to the electrode, the crystallinity of the active layer and the orientation are major factors for determining the PCE of the active layer. Furthermore, most semiconducting organic materials exhibit anisotropic charge transport whereby charge is efficiently transported in the π-stacking direction [13,14]. More recently, Tajima and Takimiya's group reported their results on surface manipulation by XRD spectral analysis. They verified that donor polymers with the face-on structure can give rise to a higher PCE due to efficient polymer chain packing [15–17].

Our group reported that in the D–π–A type polymer, poly [alkylidenefluorene-alt-di-2-thienyl-2,1,3-benzothiadiazole], steric hindrance and orientational change can occur depending on the side chain positioning. In particular, when a side chain was introduced into the spacer, an edge-on rich structure was generated with increased steric hindrance, resulting in a low PCE. In contrast, introduction of a side chain into the acceptor led to a face-on rich structure [18]. It was also confirmed that in various poly [quinacridone-alt-acceptor] molecules, when a side chain is introduced into the acceptor core, the polymer orientation is affected by the acceptor structure (type), irrespective of the position of the side chain. The study also revealed that polymers based on benzothiadiazole, quinoxaline, and dibenzo [a,c]phenazine formed edge-on structures, whereas diphenylquinoxaline-based polymers formed a face-on structure, although the side chain position changed from 6,7- to 2,3- [19–21].

All thiophene-isoindigo-based conjugated donor copolymers reported by Jian Pei's group and Wei-Fang Su's group have edge-on structures [10,22]. Frechet and coworkers achieved face-on alignment of the polymer by changing the fused phenyl ring into a thiophene moiety to reduce the torsional strain of the π-systems adjoining the isoindigo core [23].

This paper presents a method for synthesizing D–A alternating conjugated polymers (P4TI, P4TI-3, P4TI-4, P6TI-3, and P6TI-4) using 3,3′- or 4,4′-dialkyl-2,2′-bithiophene (D3 or D4) as the donor, which adopt a different side chain position from that adopted by 2,2′-bithiophene (D0), and using isoindigo-introduced thiophene and bithiophene (A1, A2) as the acceptor. XRD analysis is performed to track the structural changes of these polymers. Based on the results, we verified that the polymer arrangement can be analyzed even using UV–vis spectra. In particular, P4TI and P6TI-4 form films with face-on structures in which absorption shoulder peak is observed in the UV–vis spectra of both the solution and film states. Furthermore, the highest occupied molecular orbital (HOMO) and lowest unoccupied molecular orbital (LUMO) energy levels of the resulting polymers could be adjusted based on the difference in the electron-donating ability of the polymer donor moiety. We also verify that these polymers demonstrate a hole mobility of up to $1.07 \times 10^{-3}$ $cm^2$ $V^{-1}$ $s^{-1}$. PSCs are also fabricated by using $PC_{70}BM$ as an acceptor, and the performance of these devices is evaluated. By using P6TI-4 as the donor polymer, a photovoltaic performance (expressed as the PCE) of 3.2% at the P6TI-4:$PC_{70}BM$ (1:0.5 by weight) ratio is achieved.

## 2. Results and discussion

### 2.1. Synthesis and characterization of polymers

Scheme 1 presents the chemical structures and the common methods of synthesis of the monomers and polymers shown in Fig. 1.

The relevant monomers were synthesized by using bithiophene (D0), 3,3′-dodecylbithiophene (D3), and 4,4′-dodecyl bithiophene (D4) as donors and 6,6′-dibromo-N,N′-(2-octyldodecyl)isoindigo (A0) as the acceptor according to the methods proposed in the literature. In the case of the acceptor (A0), the 2-octyldodecyl side chain was introduced into the isoindigo core to enhance the solubility, as shown in Scheme 1.

Thiophene and bithiophene were incorporated into the spacers for the synthesis of 6,6′-bis(5-bromothiophen-2-yl)-N,N′-(2-octyldodecyl)isoindigo (A1) and 6,6′-bis(5-bromo-2,2′-bithiophen)-N,N′-(2-octyldodecyl)isoindigo (A2), respectively. To avoid steric hindrance that may arise from the introduction of the side chain, no side chain was introduced on the thiophene and bithiophene spacer moieties. The polymers were synthesized by polymerizing A1 with donors D0, D3, or D4 and A2 with donor D3 or D4 using the palladium-catalyzed Stille coupling reaction. Polymerization was performed for 48 h at 90–95 °C using toluene as the solvent, $Pd_2dba_3(0)$ as the catalyst, and tri-(o-tolyl)phosphine as the co-catalyst. Polymerization was followed by end-capping with 2-bromotihophene and 2-trimethylstannylthiophene for 3 h each. The five types of PnTI polymers, poly [thiophene moiety-alt-N,N′-(2-octyldodecyl)-6,6′-π-isoindigo] (P4TI, P4TI-3, P4TI-4, P6TI-3, and P6TI-4), obtained were re-precipitated in methanol. Purification was performed sequentially with methanol, acetone, and chloroform using a Soxhlet apparatus. Finally, the chloroform-soluble portion was re-precipitated in methanol and recovered. The obtained powders were greenish black solids with yields of 33, 67, 60, 43, and 41%. In the case of P4TI, which has a donor unit without any side chain, deposition was observed during polymerization, and the lowest yield (33%) was obtained with this polymer. P4TI dissolved only at an elevated temperature, even in common organic solvents such as THF, chloroform (CF), chlorobenzene (CB), and o-dichlorobenzene (DCB). In contrast, P4TI-3 and P4TI-4, which polymerized the donor unit by introducing a dodecyl side chain onto the 3,3′- or 4,4′-C with A1, gave rise to high yields of 67 and 60%, respectively, owing to the increased solubility. P6TI-3 and P6TI-4 also gave rise to yields of 43 and 41%, respectively, and dissolved well in the aforementioned solvents at room temperature.

The structures of the synthesized polymers were verified using $^1$H-NMR spectra (described in the ESI Figure S1). The $^1$H-NMR spectra of the polymers were similar because of the similar polymer backbones. The spectrum of P4TI had a peak at 7.74–7.30 ppm that was attributed to the hydrogen of the carbon in the aromatic phenyl of isoindigo, and the signals of the hydrogen from the 3, 4-carbon of the thiophene unit appeared at 9.50–9.28, 9.26–8.90, and 7.23–6.50 ppm. The peaks of the aromatic protons of P4TI-3 and P4TI-4 showed upfield-shifts to 7.17–7.10 and 7.18–6.38 ppm, respectively, due to the electron-shielding effect derived from the introduction of the dodecyl side chain on the 3, 4-carbon of the bithiophene donor unit. P6TI-3 and P6TI-4 were determined to have four more aromatic protons than P4TI-3 and P4TI-4 due to the introduction of bithiophene spacers. Moreover, the NMR spectra of P6TI-3 and P6TI-4 showed lower resolution and broader peaks than those of the other polymers. This is a common phenomenon in polymers having various carbon types due to the overlapping line shapes of chemical shift anisotropy [24].

Table 1 summarizes the results of the molecular weight measurements for the obtained polymers. As shown in Table 1, the number average molecular weight ($M_n$) of P4TI, P4TI-3, P4TI-4, P6TI-3, and P6TI-4 were 14, 14, 22, 13, and 17 kDa, respectively, and the corresponding polydispersity index (PDI) of each polymer was 3.94, 2.07, 2.17, 1.69, and 1.65, respectively. This reduces the planarity of the polymers by increasing steric hindrance, resulting in a decrease in the yield [18].

The thermal stability of the obtained polymers was evaluated

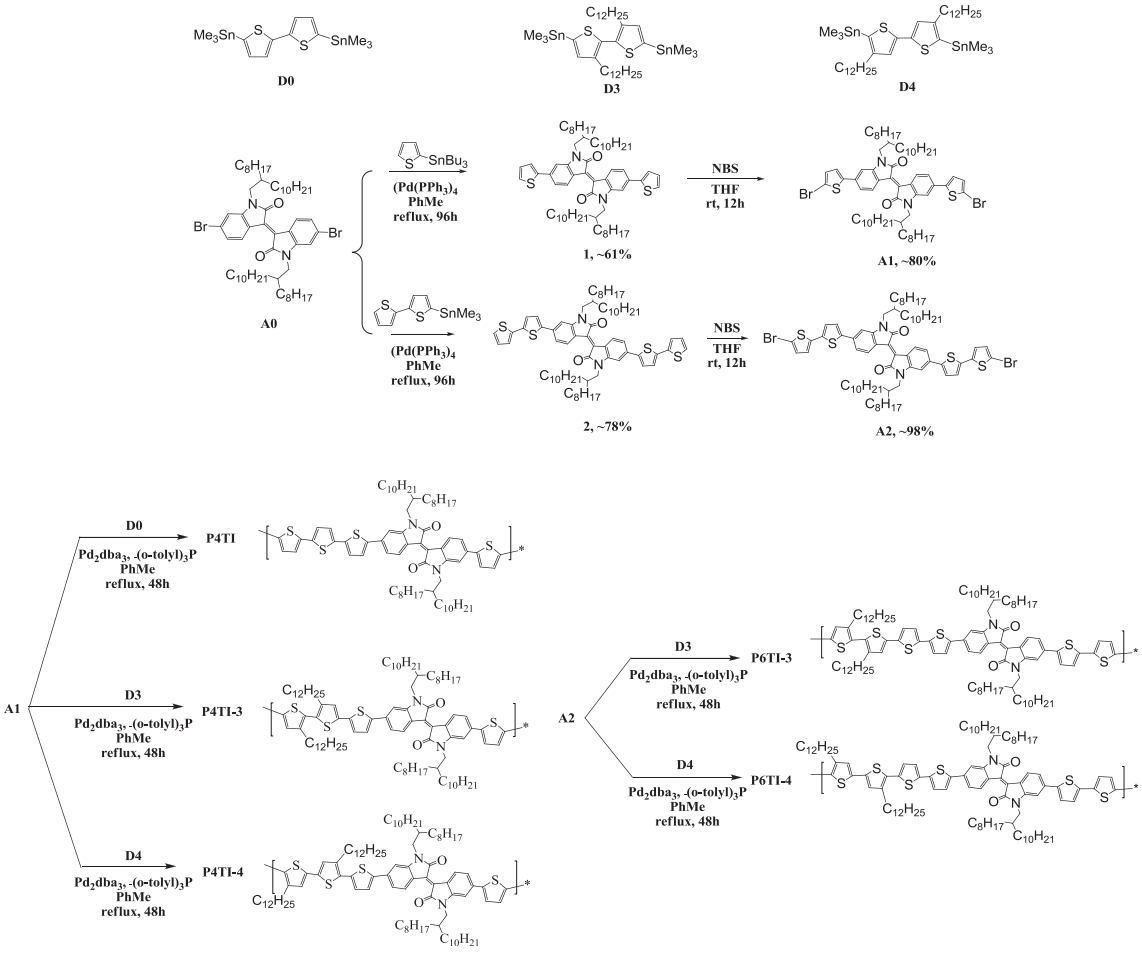


**Scheme 1.** Synthetic route to polymers.

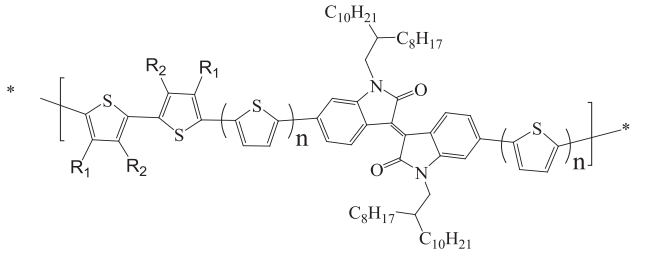


**Fig. 1.** Isoindigo-based conjugated polymers with different side chain and thienyl spacers.

using thermogravimetric analysis (TGA) and the resulting profiles are presented in the ESI (Figure S2). The TGA profiles of all the polymers revealed the temperature of 5% of the thermal weight loss in $N_2$ environment to be 318 °C or higher. All of the synthesized polymers exhibited superior thermal stability, indicative of suitability for device fabrication and application.

### 2.2. Optical properties

The UV–visible absorption of the polymers in the solution and in the film was measured to evaluate the effects of the spacer and donor side chain on the optoelectronic properties of the isoindigo-based polymers. The results are presented in Fig. 2 and Table 2.

As shown in Fig. 2, the absorption spectra of all polymers were relatively broad with onsets at 750 nm or higher (751–765 nm) and with two absorption peaks in the range of 300–800 nm. The peak in the high-energy range (400–500 nm) is ascribable to π–π*

**Table 1**
Physical and thermal properties of polymers.

| Polymer | Yield [%] | Mn[a] [kDa] | Mw[a] [kDa] | PDI[a] | Degree of polymerization[b] | $T_d$ [°C] |
|---|---|---|---|---|---|---|
| P4TI | 33 | 14 | 58 | 3.94 | 12 | 325 |
| P4TI-3 | 67 | 14 | 29 | 2.07 | 9 | 394 |
| P4TI-4 | 60 | 22 | 49 | 2.17 | 15 | 344 |
| P6TI-3 | 43 | 13 | 22 | 1.69 | 8 | 318 |
| P6TI-4 | 41 | 17 | 28 | 1.65 | 10 | 384 |

[a] Determined by GPC in tetrahydrofuran (THF) using polystyrene standards.

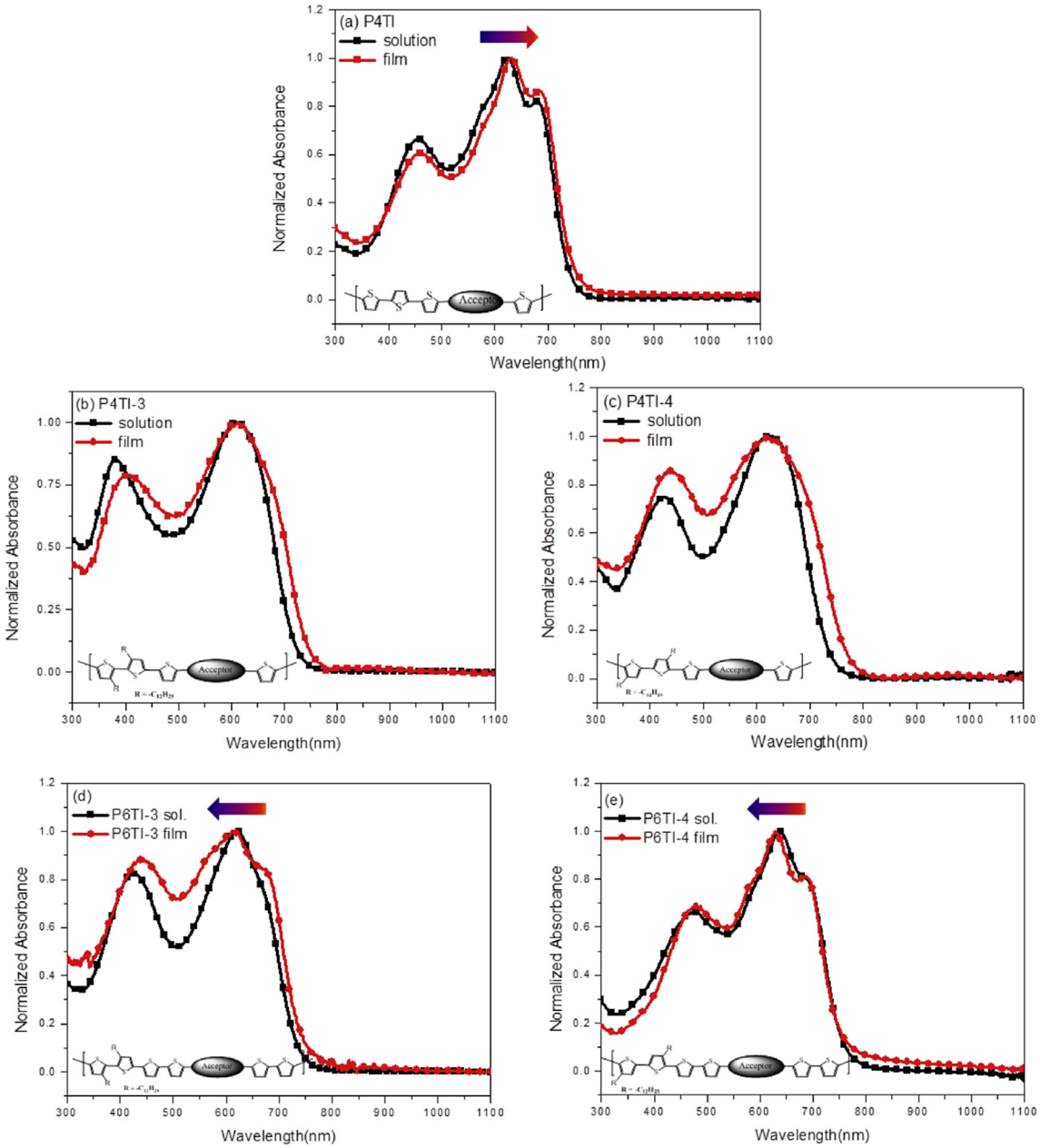


**Fig. 2.** UV–vis absorption spectra of polymers in solution and film: (a)P4TI, (b)P4TI-3, (c) P4TI-4, (d) P6TI-3, (e) P6TI-4.

transition of the donor segments (oligothiophene group), and the peak in the low-energy range (600–750 nm) is ascribed to the intramolecular charge transfer (ICT) transition between the donor and the acceptor [25].

In the solution state, as illustrated in Table 2, all polymers exhibited similar maximum-absorption peaks ($\lambda_{max}$ = 610–638 nm). Additionally, these polymers had similar molar absorption coefficients ($\varepsilon_{max} = 3.8 \times 10^4$–$5.0 \times 10^4$ $M^{-1}$ $cm^{-1}$) as presented in ESI Figure S3. P6TI-4, despite its low molecular weight (Mn = 17 kDa, Mw = 28 kDa), had a higher molar absorption coefficient ($\varepsilon_{max} = 5.0 \times 10^4$ $M^{-1}$ $cm^{-1}$) than P4TI-4 (Mn = 22 kDa, Mw = 49 kDa). In the film state, all polymers had a low optical band gap ($E_g$) of 1.62–1.66 eV, as calculated from $E_{onset}$ (746–765 nm) [26].

However, the characteristics of the absorption peaks (600–750 nm) that induced the ICT transition were observed to be dependent on the donor side chains and spacers. In both the solution and film, the UV–vis absorption spectra of P4TI and P6TI-4 exhibited absorption shoulder peaks at $\lambda_{sh}$ = 680 and 690 nm and $\lambda_{sh}$ = 683 and 687 nm, respectively. Shoulder absorption peaks are caused by polymer-chain stacking, which implies that polymers that exhibit shoulder absorption peaks have more intensive intermolecular interactions than those that do not [27,28]. In particular, P4TI and P6TI-4 were verified to have a strong aggregation or orderly π-π stacking among their polymer chains, even in dilute solution [29,30]. But, for P4TI-3 and P4TI-4, in which the side chains are connected to the donors, no absorption shoulder peaks were observed in either the solution or the film. This is attributed to weakened inter-chain interactions in these polymers due to the introduction of the side chains. The absorption spectra of P4TI-3 were blue-shifted by 15 and 19 nm in the solution and in the film, respectively, relative to those of P4TI. The absorptions of P4TI-4 were also blue-shifted by 4 and 12 nm in the solution and in the

**Table 2**
Optical and electrochemical data of polymers.

| Polymer | UV–vis absorption | | | | | $E_g^{op}$,[a] [eV] | Cyclic voltammetry | | |
|---|---|---|---|---|---|---|---|---|---|
| | $CHCl_3$ solution [nm] | | Film [nm] | | | | $E_{ox}^{onset}$ [V] | HOMO[b] [eV] | LUMO[c] [eV] |
| | $\lambda_{max}$ [nm] | $\lambda_{sh}$ [nm] | $\lambda_{max}$ [nm] | $\lambda_{sh}$ [nm] | $\lambda_{onset}$ [nm] | | | | |
| P4TI | 625 | 456, 680 | 633 | 456, 690 | 765 | 1.62 | 0.98 | −5.33 | −3.71 |
| P4TI-3 | 610 | 381 | 614 | 406 | 746 | 1.66 | 1.31 | −5.67 | −4.01 |
| P4TI-4 | 621 | 426 | 621 | 437 | 764 | 1.62 | 0.89 | −5.23 | −3.66 |
| P6TI-3 | 620 | 425 | 614 | 440, 676 | 751 | 1.65 | 1.12 | −5.33 | −3.68 |
| P6TI-4 | 638 | 474, 683 | 630 | 477, 687 | 751 | 1.65 | 0.80 | −5.14 | −3.49 |

[a] Calculated from the intersection of the tangent on the low energetic edge of the absorption spectrum with the baseline.
[b] $E_{HOMO} = -[E_{onset(vs\ Ag/AgCl)} - E_{1/2(Fc/Fc+\ vs\ Ag/AgCl)}] - 4.8$ eV.
[c] LUMO = HOMO + $E_g$.

film, respectively. These reductions in the absorption region are attributable to an increase in the electron-donating property of the polymers induced by the introduction of side chains. This may be explained by the fact that the decreased ICT effect between the donor and acceptor segments leads to a reduction in the electron-withdrawing effect of the isoindigo segments [31]. The absorption region was blue-shifted more for P4TI-3 than for P4TI-4 because of the change in the conjugation length of the main chain due to the difference in the tilt angle depending on the side chain position. However, for P6TI-3 in which bithiophene is introduced into the spacer, no absorption shoulder peaks were apparent in the solution absorption spectrum, whereas a shoulder peak was apparent for the film ($\lambda_{sh} = 676$); this is in contrast with P6TI-4 and P4TI-3 that showed absorption shoulder peaks in both states and neither state, respectively. This is attributed to the increased conjugation length as a result of extended electronic delocalization mediated by the bithiophene introduced into the spacer compared to thiophene. In other words, the bithiophene spacer resulted in a polymer main chain with a more planar conformation between the donor unit and isoindigo acceptor unit than was achieved with the thiophene spacer, and thus induced orderly π-π stacking. This result is in good agreement with greater extension of the absorption range ($\lambda_{onset}$ = 746 → 751 nm) and band gap reduction ($E_g = 1.66 \rightarrow 1.65$ eV) achieved with P6TI-3 compared with P4TI-3 [29,32].

The UV–visible spectra of the polymers in the film were different from that in the solution depending on the type of spacer. Although the spectra of P4TI, P4TI-3, and P4TI-4 that had thiophene spacers were red-shifted (8 nm, 4 nm, 0 nm, respectively) for the film when compared with the solution state, P6TI-3 and P6TI-4 that had bithiophene spacers exhibited a blue-shift (6 nm and 8 nm, respectively). These results lead to the confirmation that the side chain position and spacer length have a significant impact on the planarity of the polymer main chain.

### 2.3. X-ray diffraction (XRD) measurement

To better understand the characteristics of the polymer chemical structure and thin-film ordering and crystallinity, XRD measurements were performed on samples treated at annealing temperatures.

Figure S4(a) presents the XRD profiles of the polymer thin films measured in the out-of-plane mode for evaluation of the ordering structure.

The XRD spectra of the P4TI and P6TI-4 thin films measured in the out-of-plane mode showed diffraction peaks at 5.04°, 22.66° and 3.68°, 19.09–23.38°, respectively. This suggests that the polymers form the (h00) lamellar structure and (0h0) lamellar structure simultaneously. When a π-π stacking peak is observed for the (010) plane in the out-of-plane mode, it is highly probable that the polymer thin film adopts a crystalline form with face-on orientation. This can be verified by acquiring XRD data in the in-plane mode. The results of a calculation using Bragg's law ($\lambda = 2d\sin\theta$) indicated that the highly ordered (100) lamellar d-spacings ($d_l$) were 17.53 and 24 Å, respectively, and the π-π stacking distances ($d_\pi$) were 3.92 and 4.67–3.70 Å, respectively. However, unlike the P4TI thin film, for the P4TI-3 thin film had very weak intensity of XRD spectra. The peak intensity of the (h00) diffraction peak for P4TI-3 is negligible and close to the baseline level, P4TI-3 forms almost amorphous thin film. And P4TI-4 thin film only the (h00) diffraction peak was observed at 3.92° and the (0h0) peak could not be observed. This indicates that this polymer form an edge-on orientation aligned perpendicularly to the substrate. Calculations of the d-spacing ($d_1$) for the P4TI-4 thin film gave values of 22.54 Å which is larger than the value for P4TI. This is in good agreement with the observation that the shoulder peaks disappeared in the UV–vis absorption spectra due to the weakened intermolecular interactions. The (h00) diffraction peak was not observed for P6TI-3, and only the (010) diffraction peak was observed at 18.98°. The $d_\pi$ value calculated for P6TI-3 was 4.67 Å. To determine the crystal structure of the P4TI, P6TI-3 and P6TI-4 thin films, the XRD patterns were acquired in the in-plane mode.

Figure S4(b) presents the XRD profiles of the P4TI, P6TI-3, and P6TI-4 polymer thin films measured in the in-plane mode. The XRD profile for P4TI in the in-plane mode had one diffraction peak at low angle, which suggests that the polymer thin film formed a face-on structure. P6TI-3 showed one broad diffraction peak at high ($2\theta = 15°–20°$) angles, which suggests that the polymer thin film formed an edge-on structure. The thin film of P6TI-4 showed XRD peaks at both low and high angles in the in-plane mode, demonstrating that this crystal structure had a bimodal orientation; however, the sharp diffraction peak at approximately 5° had a higher intensity than the broad peak at 20–25°, thus confirming that the face-on structure was predominant within the bimodal thin film [16]. In studies by Jian Pei and Wei-Fang Su's groups, all of the evaluated thiophene-isoindigo copolymers adopted the edge-on conformation on the substrate [10,22]. This is consistent with the present observations for P4TI-3, P4TI-4, and P6TI-3, for which dodecyl side chains were introduced into the respective donor moieties. This is because the introduction of the side chain increased the tilt angle between the donor and spacer and the tilt angle inside the donor unit to 39–66° (refer to the DFT computational study).

In contrast to these polymers, P4TI formed face-on structures and P6TI-4 formed face-on rich structures. Comparison of these results with the shoulder peaks in the UV–vis absorption spectra in Fig. 2 reveals that P4TI and P6TI-4, which adopted face-on structures, exhibited shoulder peaks in solution as well as in film. P4TI-3 and P4TI-4 with edge-on structures showed shoulder peaks in neither state. In contrast, P6TI-3 with edge-on structure showed

shoulder peaks in the film, whereas no shoulder peaks were observed in the solution.

Erjun Zhou and Keisuke Tajima et al. reported that dithienopyrrole-benzothiadiazole polymers with no absorption shoulder peaks had amorphous structures, indicated by the absence of defined XRD peaks; however, those with shoulder peaks in the absorption spectra had crystalline structures based on XRD [33]. Keisuke Tajima and coworkers reported that the UV spectra of the diketopyrrolopyrrole-oligothiophene polymers differed based on the types of side chains introduced, where the clearest shoulder peaks in the solution and in the film were observed for polymers with −OH groups; these polymers were verified to have face-on structures based on the analysis of the in-plane XRD patterns [34]. Thus, polymers for which shoulder peaks are observed in the UV–vis absorption spectrum in both the solution and in film undergo aggregation among the main chains and π-π stacking and strongly tend towards face-on orientation.

### 2.4. Electrochemical properties

Fig. 3 presents the cyclic voltammograms (CV) of the thin films of the synthesized polymers. CVs were measured to investigate the effects of varying donor segments and spacers on the optoelectronic properties. CV measurements were performed using 0.1 M tetrabutylammonium-hexafluorophosphate (TBAHFP) in acetonitrile solution. The cyclic voltammograms of the polymers exhibit reversible oxidation/reduction behavior, and the HOMO energy levels of the polymers were calculated using ferrocene (Fc) as the internal standard, where $\{E_{HOMO}\ (eV) = -4.8 - (E_{onset} - E_{1/2(Ferrocene)})\}$. The LUMO energy level was calculated by obtaining the difference between the optical band gaps and the HOMO energy level. These results are summarized in Table 2.

The oxidation onset potentials ($E^{ox}_{onset}$) of P4TI, P4TI-3, P4TI-4, P6TI-3, and P6TI-4 were +0.98, +1.31, +0.89, +1.12, and +0.80 V, respectively. Their calculated HOMO levels were −5.33, −5.67, −5.23, −5.33, and −5.14 eV, respectively. The P4TI, P4TI-3, and P6TI-3 polymers had low HOMO levels below −5.27 eV, which indicates superior oxidative stability [35].

The calculation results indicated that the HOMO energy levels of the polymers tended to increase in proportion to the increase in the electron-donating property and conjugation length of the donor segments. The introduction of side chains into the donor segments gave rise to a 0.1 eV increase in the HOMO level for P4TI-4 due to the increased electron-donating ability relative to P4TI. However, the HOMO level of P4TI-3 decreased relative to P4TI. This can be attributed to the reduced electron-donating activity caused by the disrupted conjugation resulting from the large tilt angle inside the D3 donor, which weakened the donor ability of the D3 to below that of the D0 donor, thereby lowering its HOMO level. Additionally, the respective HOMO levels of P6TI-3 and P6TI-4 that had bithiophene spacers were up-shifted by 0.34 and 0.09 eV relative to the HOMO levels of P4TI-3 and P4TI-4, which was driven by the increase in the electron-donating properties of P6TI-3 and P6TI-4. These results are consistent with those reported by You et al. in which the HOMO energy level were found to be dependent on the donor strength in the push–pull system [5]. The introduction of a side chain on the donor unit, increasing the number of spacers, and increasing the coplanarity were found to be favorable conditions for increasing the donor strength. This is also in line with reports by Lidzey et al. that verified an increase in the HOMO level in proportion to the increase in the electron-donating properties of thiophene [36,37].

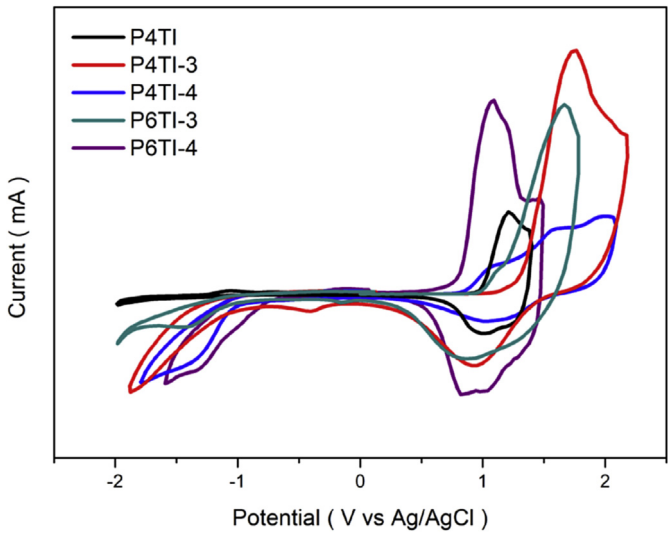


**Fig. 3.** Cyclic voltamograms of polymers.

### 2.5. Computational study of polymers

Density functional theory (DFT) simulations were performed to understand the electrical properties, molecular geometries and electron density of states of the polymers. Gaussian 09 with the hybrid B3LYP correlation functional and split valence 6–31G(d) basis set was used for the DFT calculation. Oligomers with two repeating units were selected for the calculation. The calculated HOMO and LUMO orbitals are shown in Fig. 4 and Table 3.

The HOMOs are delocalized over the polymer main chains, whereas the LUMOs are localized on the acceptor indigo dye. This is due to the structural features of the quinoid formed between the non-bonding electron pairs on nitrogen and sulfur that exhibit electron-withdrawing characteristics [38].

As shown in Table 3, the HOMO levels determined from the DFT calculations tended to increase with the introduction of side chains on the P4TI (−4.86 eV) backbone or elongation of the spacer lengths (P4TI: −4.86 eV; P4TI-4: −4.84 eV, P6TI-4: −4.76 eV). This is in agreement with the CV measurements in which the HOMO level increased as the electron-donating ability of the donor unit increased (Table 2). Interestingly, we observed that differences in the positions of the side chains introduced into the donors resulted in different HOMO levels. The polymers with the D3 unit (P4TI-3 and P6TI-3) had lower HOMO levels (−4.99 and −4.85 eV, respectively) than those (−4.84 and −4.76 eV) of the polymers with the D4 unit (P4TI-4 and P6TI-4, respectively). This is due to the difference in the 2, 2′-C tilt angles in the respective donor segments, as shown by the calculation side views shown in Fig. 4 in which the tilt angles (66.55° and 59.5°) of the polymers with the D3 unit (P4TI-3 and P6TI-3, respectively) are observed to be larger than those (15.14 and 11.73°) of the polymers with the D4 unit (P4TI-4 and P6TI-4, respectively). Therefore, the position in which the side chain is introduced on the donor unit plays a decisive role in determining

**Table 3**
Calculated parameters.

| Polymer | Dihedral angle (deg) | | | $HOMO^{cal.}$[eV] | $LUMO^{cal.}$[eV] |
|---|---|---|---|---|---|
| | 1 | 2 | 3 | | |
| P4TI | 15.94 | 20.50 | 21.36 | −4.86 | −2.87 |
| P4TI-3 | 14.68 | 22.11 | 21.78 | −4.99 | −2.83 |
| P4TI-4 | 39.37 | 22.58 | 21.07 | −4.84 | −2.81 |
| P6TI-3 | 16.47 | 22.07 | 21.69 | −4.85 | −2.84 |
| P6TI-4 | 14.72 | 21.05 | 21.07 | −4.76 | −2.84 |

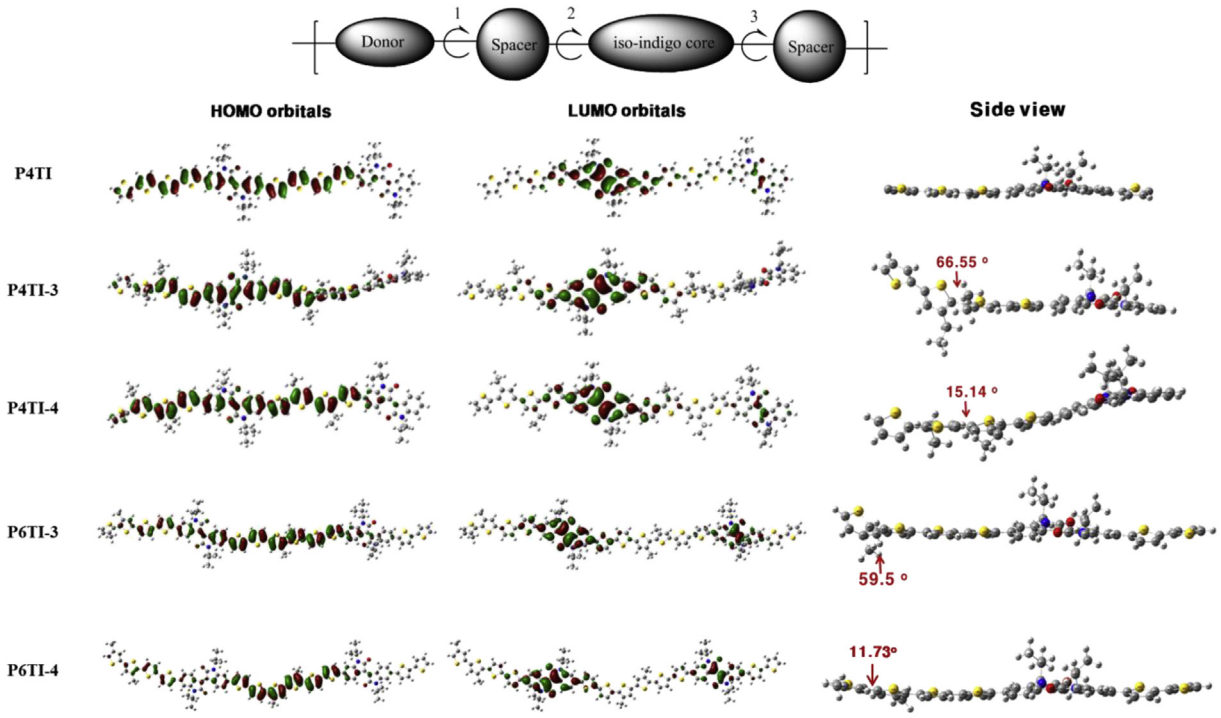


**Fig. 4.** The calculated LUMO and HOMO orbitals for monomer unit and the dimermodels of polymers.

the HOMO energy level. In the case of P4TI, the introduction of the side chain on 3-C, rather than on 4-C, disrupts conjugation in the bithiophene unit. This curtails the electron-donating activity of P4TI-3 and P6TI-3 and results in the lower HOMO level and the decrease in the absorption region due to the shortening of the conjugation length compared to P4TI-4 and P6TI-4 [39].

The dihedral angles, 2 and 3, between the two spacer groups and the isoindigo core were similar (20.50°–22.58°) for all polymers. However, in the case of P4TI-4, the dihedral angle 1, between the core acceptor and donor was as large as 39.37°, which is approximately 20° larger than the other polymers. This difference arises from positioning of the side chain of D4 closer to the acceptor, thus inducing a strong steric hindrance with the bulky 2-octyldodecyl side chain of isoindigo and expanding the dihedral angle, 1. Although the D4 unit is also present in P6TI-4, steric hindrance was mitigated using bithiophene for mediating elongation of the spacer length. This expanded the distance between the donor and acceptor, decreased the dihedral angle, 1 (14.72°), in the P6TI-4 to 37% of P4TI-4, thus indicating a high planarity of the overall structure. The strong steric hindrance leads to a decrease in intermolecular π-π stacking and disruptive conjugation, thus reducing charge transport [40]. Additionally, the increase in the tilt angle breaks the conjugation and diminishes the current. It is therefore expected that the current of the P6TI-4 and P4TI polymers that have a small tilt angle will keep a high $J_{SC}$ during the OPV cell production.

### 2.6. Photovoltaic properties

To evaluate the photovoltaic (PV) properties of the synthesized polymers, BHJ PSC devices were fabricated with ITO/PEDOT:PSS/polymer:$PC_{70}BM$/$BaF_2$/Ba/Al structures. All of the fabricated devices were encapsulated inside a glove box. The J-V characteristics of the devices were measured under ambient atmosphere at an active area of 4 $mm^2$. The weight ratio of Polymer:$PC_{70}BM$ in the devices was varied as follows: 1:0.5, 1:1, and 1:2. Dichlorobenzene (DCB) was used as the solvent. The ratio of polymer to $PC_{70}BM$ optimized condition was 1:1(P4TI, P4TI-4), 1:2(P4TI-3, P6TI-3) and 1:0.5(P6TI-4). The four individual devices were tested under various conditions. Table 4 and Table S1 summarize the photovoltaic response data including $V_{OC}$, $J_{SC}$, FF, and PCEs. The J-V curves at the optimized weight ratios of the polymers are presented in Fig. 5 (a), and the resulting IPCE is shown in Fig. 5 (b).

As indicated in Table 4, the $J_{SC}$ of P4TI was higher (6.7 mA/$cm^2$) than the other polymers, and the open circuit voltage ($V_{oc}$ = 0.82 V) of P4TI was also moderately high. However, the limited solubility of this polymer was reflected in the low fill factor (FF) of 48.9%, and

**Table 4**
Photovoltaic properties of polymers.

| Polymer | Device structure | Solvent + additive | $PC_{70}BM$ ratios | Voc[V] | Jsc[mA/$cm^2$] | FF[%] | PCE[%] |
|---|---|---|---|---|---|---|---|
| P4TI | conventional | ODCB + none | 1: 1 | 0.82 | 6.7 | 48.9 | 2.8 |
| P4TI-3 | conventional | ODCB + none | 1: 2 | 0.92 | 1.3 | 38.9 | 0.48 |
| P4TI-4 | conventional | ODCB + none | 1: 1 | 0.82 | 1.6 | 46.4 | 0.61 |
| P6TI-3 | conventional | ODCB + none | 1: 2 | 0.82 | 5.6 | 39.7 | 1.8 |
| P6TI-4 | conventional | ODCB + none | 1: 0.5 | 0.76 | 6.3 | 67.1 | 3.2 |
| P6TI-4 | conventional | CB + DIO | 1: 2 | 0.66 | 6.4 | 63.3 | 2.8 |
| P6TI-4 | inverted | CB + DIO | 1: 2 | 0.70 | 7.2 | 66.0 | 3.5 |

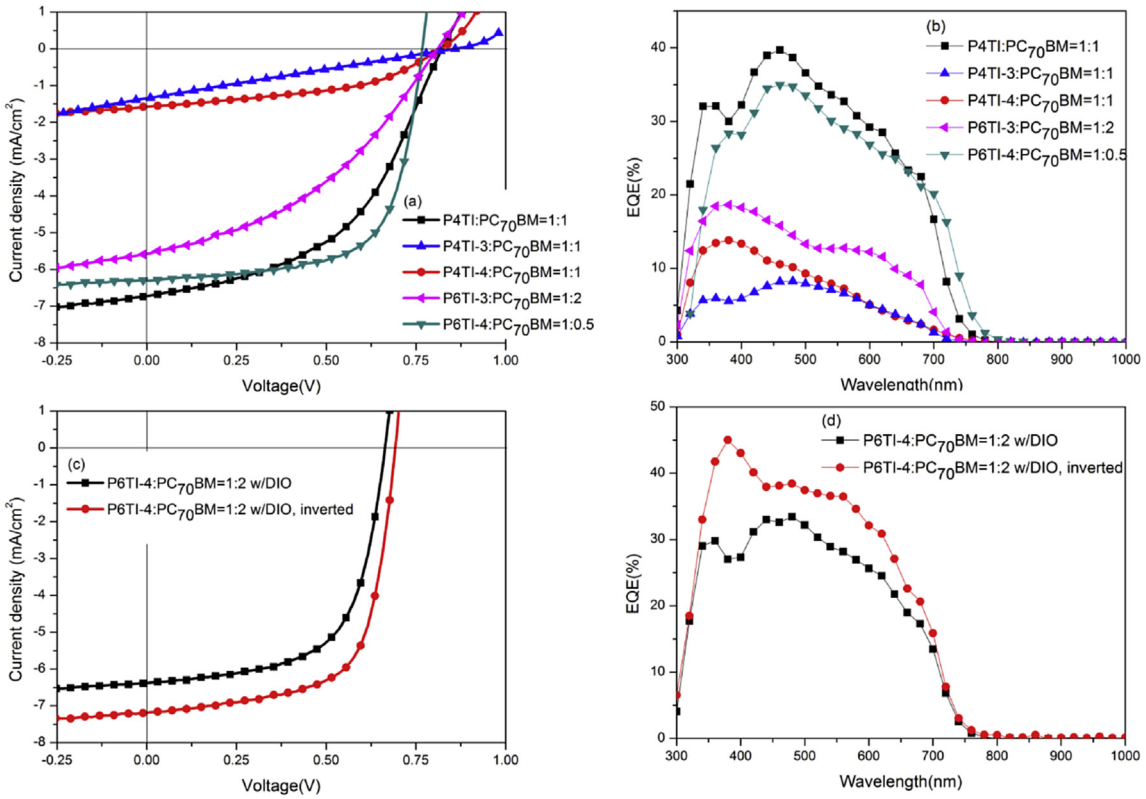


**Fig. 5.** The J–V curves of the PSC based on polymer: $PC_{70}BM$ (a), (b) under the illumination of AM 1.5G, 100 mW/cm$^2$. The IPCE spectra (c), (d).

led to a rather low PCE (2.8%). In contrast, despite its low $V_{OC}$ (0.76 V) due to the high HOMO level (−5.14 eV), the P6TI-4 exhibited a high FF (67.1%) because of its superior solubility and H-stacked face-on structure, resulting in a higher PCE of 3.2%. Low FF indicates strong recombination in the OPV cells. There have been several efforts to improve the transport property of BHJ OPV by controlling its morphology [41]. The polymer solubility is basic property to influence not only the processability and morphology, but also physical polymer properties such as phase behavior, structural order and charge transport properties [42]. These two polymers were evaluated as having planar and face-on rich structures based on the XRD analysis (Figure S4). However, P4TI-3 and P4TI-4 that had edge-on structures and large tilt angles had a low $J_{SC}$ (1.3 and 1.6 mA/cm$^2$, respectively). Notably, the highest open circuit voltage (0.92 V) and deepest HOMO level (−5.67 eV) were observed for P4TI-3 due to the weakened conjugation induced by the large internal tilt angle of this polymer. Nevertheless, P4TI-3 and P4TI-4 had PCEs as low as <1%. In contrast, despite its edge-on structure and the large tilt angle of the donor unit, the $J_{SC}$ of P6TI-3 was higher (5.6 mA/cm$^2$) than for P4TI-3. This is due the differences in their stacking patterns (while P4TI-3 forms a J-stacked structure, P6TI-3 forms an H-stacked structure, which induces parallel aggregation). But, the PCE of P6TI-3 did not exceed 1.8% due to its low FF (39.7%).

The devices fabricated with these polymers exhibited adequately broad and large EQE values in the absorption spectral range of 300–750 nm with a decline at wavelengths above 750 nm. In particular, the P4TI:$PC_{70}BM$ blend-based devices exhibited a high EQE (up to 39.7%) at 460 nm, and this is consistent with the highest photo-current achieved with these devices [43].

To optimize and enhance the performance of P6TI-4 device, 3 vol% 1,8-diiodooctane(DIO) was add as solvent additive. However, the PCE was not increased by the additive. Compared with conventional OPVs, inverted type devices can also take advantage of the vertical phase separation and concentration gradient in the active layer, which is naturally self-encapsulated because air-stable metals are used as the top electrode [44]. So we manufactured inverted PSC devices with ITO/ZnO/P6TI-4:$PC_{70}BM$/$MoO_3$/Ag structures, PCE is increased to 3.5%. It showed slightly increased a Jsc, from 6.3 to 7.2 mA/cm$^2$.

### 2.7. Charge carrier mobility and morphology analysis

The space charge limited current (SCLC) model based on the Poole–Frenkel Law was used to determine the hole mobility in polymers and blends containing polymers and $PC_{70}BM$. The graphs are described in the ESI* (Figure S5–S14, Table 5).

P4TI and P6TI-4 blend films, which formed face-on crystallites, exhibited the highest hole mobilities with values of $2.15 \times 10^{-2}$ and $5.80 \times 10^{-2}$ cm$^2$(V$^{-1}$ s$^{-1}$), respectively. P4TI and P6TI-4 blend films had high hole mobility and produced the highest $J_{SC}$ in the fabricated photovoltaic cells. P4TI-3 and P4TI-4 blend films, in which side chains were introduced into the donors, exhibited the lowest hole mobilities of $5.64 \times 10^{-4}$ and $6.08 \times 10^{-4}$ cm$^2$(V$^{-1}$ s$^{-1}$), respectively. This is due to the decrease in the conjugation length induced by the large intermolecular tilt angle. The associated decrease in the carrier mobility led to a low $J_{SC}$ of the fabricated photovoltaic cells (1.3 and 1.6 mA/cm$^2$, respectively). P6TI-3 blend film that had the bithiophene spacer exhibited a higher hole mobility ($4.03 \times 10^{-3}$ cm$^2$(V$^{-1}$ s$^{-1}$)) than P4TI-3 despite the large tilt angle within the donor unit of P6TI-3. This is consistent with the $J_{SC}$ of photovoltaic cells fabricated with this polymer.

Based on the linear fitting between $\ln(JL^3/V^2)$ and $(V/L)^{0.5}$ for the hole only SCLC, the zero-field hole mobility of P4TI, P4TI-3, P4TI-4, P6TI-3 and P6TI-4 can be calculated to be $1.89 \times 10^{-2}$, $3.59 \times 10^{-4}$, $4.87 \times 10^{-4}$, $3.53 \times 10^{-3}$ and $3.89 \times 10^{-2}$ cm$^2$(V$^{-1}$ s$^{-1}$), respectively.

**Table 5**
Hole mobility of polymers and polymers blended with $PC_{71}BM$.

| Polymer | $PC_{71}BM$ ratios (w:w) | Film thickness [nm] | Hole mobility [$cm^2(V^{-1}\ s^{-1})$] |
|---|---|---|---|
| P4TI | 1: 1 | 56.7 | $2.15 \times 10^{-2}$ |
| P4TI-3 | 1: 1 | 34.3 | $5.64 \times 10^{-4}$ |
| P4TI-4 | 1: 1 | 35 | $6.08 \times 10^{-4}$ |
| P6TI-3 | 1: 2 | 13.6 | $4.03 \times 10^{-3}$ |
| P6TI-4 | 1: 0.5 | 19.7 | $5.80 \times 10^{-2}$ |
| P4TI | none | 55.9 | $1.89 \times 10^{-2}$ |
| P4TI-3 | none | 38.7 | $3.59 \times 10^{-4}$ |
| P4TI-4 | none | 45.7 | $4.87 \times 10^{-4}$ |
| P6TI-3 | none | 27.9 | $3.53 \times 10^{-3}$ |
| P6TI-4 | none | 28.1 | $3.89 \times 10^{-2}$ |

The carrier mobilities of the polymer:$PC_{70}BM$ blend films are only slightly higher than that of neat polymer films.

The surface morphology of polymer blends is also a critical factor influencing the performance of PSCs. Therefore, the morphologies of the polymer:PCBM blend films were evaluated via AFM as illustrated in Figure S15. The dark-colored and light-colored areas correspond to PCBM domains and polymers, respectively [45]. The surface of the P6TI-4:$PC_{70}BM$ blend film with a FF = 67.1% was smooth with nanoscale features and the root-mean-square (RMS) roughness was approximately 1.94 nm. In contrast, black dots were observed in the AFM images of the P4TI, P4TI-3, P4TI-4, and P6TI-3:$PC_{70}BM$ blend films due to large aggregate PCBM domains. The P4TI:$PC_{70}BM$ blend film had a high RMS roughness of 5.61 nm due to its low solubility. When side chains were introduced into the donors of the P4TI, P4TI-3 and P4TI-4:$PC_{70}BM$ blend films exhibited higher RMS roughness due to the polymer chain tilt compared to P4TI. In particular, the P4TI-3 blend film that employed D3 as a donor induced intensive phase separation, and its RMS roughness was as large as 7.04 nm. The phase separation in the active layer lowered the FF to 36.3% for the fabricated photovoltaic cells and increased the charge recombination, thus reducing the charge transport rate and Jsc. P6TI-3, which employed the bithiophene spacer, had a lower RMS roughness (6.73 nm) compared to P4TI-3. This is in good agreement with the reduced tilt angle between the donor unit and the acceptor unit.

## 3. Experimental

### 3.1. Materials

All starting materials were purchased from Sigma Aldrich and Alfar Aesar, and used without further purification. Toluene and tetrahydrofuran (THF) were distilled from benzophenone ketyl and sodium. The following compounds were synthesized following modified literature procedures: 2,5-bis(trimethylstannyl)-2,2′-bithiophene (D0) [46], 3,3′-didodecyl-2,2′-bithiophene-5,5′-diyl) bis(trimethylstannane) (D3) [47], (4,4′-didodecyl-2,2′-bithiophene-5,5′-diyl)bis (trimethylstannane) (D4) [48], 6,6′-dibromo-N, N′-(2-octyldodecyl)isoindigo (A0) [49], 2T [50].

#### 3.1.1. N, N′-(2-octyldodecyl)-6, 6′-dithiphen-2-yl-isoindigo (1)

To the solution of A0 (5.5224 g, 5.634 mmol) and 2-(tributylstannyl)thiophene (4.836 g, 13.22 mmol) in toluene (47 mL), tetrakis(triphenylphospine)palladium(0) ($Pd(PPh_3)_4$) (0.26 g) were added in one portion. The mixture was stirred under reflux 96 h. Then the mixture was cooled to room temperature and poured into water. The organic phase was extracted by diethyl ether, and then washed with water, dried over $MgSO_4$. After the removal of the solvent under reduced pressure, the solids were purified by silica chromatography with dichloromethane: hexane = 2:3. Yield (3.4 g, 61%) $^d$H (400 MHz; $CDCl_3$; $Me_4Si$): 9.19 (d, 2H), 7.43 (d, 2H), 7.37 (d, 2H), 7.32 (d, 2H), 7.16–7.11 (m, 2H), 7.00 (s, 2H), 3.72 (d, 4H), 1.95 (m, 2H), 1.46–1.19 (br, 48H), 0.89–0.83 (br, 12H).

#### 3.1.2. N, N′-(2-octyldodecyl)-6, 6′-di-2,2′-bithiphen-5-yl-isoindigo (2)

2 was synthesized with the same procedure of 1. To the solution of A0 (1.8 g, 1.83 mmol) and 5-(tributylstannyl)-2,2′-bithiophene (1.483 g, 4.507 mmol) in toluene (15 mL), tetrakis(-triphenylphospine)palladium(0) ($Pd(PPh_3)_4$) (0.086 g) were added in one portion. The mixture was stirred under reflux 96 h. Then the mixture was cooled to room temperature and poured into water. The organic phase was extracted by diethyl ether, and then washed with water, dried over $MgSO_4$. After the removal of the solvent under reduced pressure, the solids were purified by silica chromatography with dichloromethane: hexane = 2:3. Yield (1.681 g, 78.2%) $^d$H (400 MHz; $CDCl_3$; $Me_4Si$): 9.19 (d, 2H), 7.32–7.17 (m, 10H), 7.07–7.03 (m, 2H), 6.92 (s, 2H), 3.78 (d, 4H), 1.90 (m, 2H), 1.36–1.22 (br, 48H), 0.85–0.83 (br, 12H).

#### 3.1.3. N, N′-(2-octyldodecyl)-6, 6′-di(5-bromothiophen-2-yl)-isoindigo (A1)

To a solution of 1 (1.92 g, 1.94 mmol) in 58 mL THF, NBS (0.725 g, 4.07 mmol) was added portionwise in 2 h in the dark. The reaction mixture was stirred at room temperature for 12 h. Then it was poured into water and extracted with diethyl ether. Removal of the solvent and column purification on silica gel using dichloromethane:hexane = 1:2. Yield (1.78 g, 80%) $^d$H (400 MHz; $CDCl_3$; $Me_4Si$): 9.19 (d, 2H), 7.20–7.15 (m, 4H), 7.07 (d, 2H), 6.87 (s, 2H), 3.70 (d, 4H), 1.90 (m, 2H), 1.42–1.19 (br, 48H), 0.86–0.83 (br, 12H).

#### 3.1.4. N, N′-(2-octyldodecyl)-6, 6′-di(5-bromo-2,2′-bithiophen-2-yl)-isoindigo (A2)

A2 was synthesized with the same procedure of A1. To a solution of 2 (1.68 g, 1.46 mmol) in 44 mL THF, NBS (0.52 g, 2.92 mmol) was added portionwise in 1 h in the dark. The reaction mixture was stirred at room temperature for 12 h. Then it was poured into water and extracted with diethyl ether. Removal of the solvent and column purification on silica gel using dichloromethane:hexane = 1:2. Yield (1.88 g, 98.3%) $^d$H (400 MHz; $CDCl_3$; $Me_4Si$): 9.15 (d, 2H), 7.29–7.25 (d, 4H), 7.10–7.09 (d, 2H), 6.99–6.95 (m, 4H), 6.89 (s, 2H), 3.68 (d, 4H), 1.90 (m, 2H), 1.41–1.22 (br, 48H), 0.87–0.83 (br, 12H).

### 3.2. General polymerizations

To a mixture of tris(dibenzylideneacetone)dipalladium(0) ($Pd_2dba_3$) (9.52 mg, 0.0104 mmol, 4 mol%), tri-(o-tolyl)phosphine (12.66 mg, 0.0416 mmol, 16 mol%), stannane compound (0.26 mmol, e.g. D0, D3 and D4) and equivalent of halogen compound (e.g. A1 and A2) were dissolved in 10 mL of degassed toluene. The mixture was vigorously stirred at 90–95 °C for 48 h under the nitrogen. After 48 h, 2-bromotihophene was added to the reaction, 3 h after which 2-trimethylstannylthiophene was added and the reaction refluxed for 3 h to complete the end-capping reaction. After the mixture was cooled to room temperature, poured into methanol and filtered. The filtered polymer was further dissolved in $CHCl_3$ and reprecipitated into methanol and filtered. The polymer was further purified by washing methanol and acetone, respectively, in a Soxhlet apparatus for 24 h. The chloroform part was reprecipitated with methanol and filtrated then, dried under reduced pressure at 50 °C.

*3.2.1. Poly[2,2′-bithiophene-alt-N, N′-(2-octyldodecyl)-6, 6′-dithiphen-2-yl-isoindigo] (P4TI)*

Greenish black solid, 0.099 g (yield = 33%). $^1$H NMR (400 MHz, $CDCl_3$, d): 9.50–9.28 (m, 2H), 9.26–8.90 (m, 2H), 7.74–7.30 (m, 6H), 7.23–6.50 (m, 4H), 3.82–3.38 (m, 4H), 2.58–2.41 (m, 4H), 2.05–1.76 (m, 8H), 1.49–0.98 (m, 52H), 0.98–0.69 (m, 12H).

*3.2.2. Poly[3,3′-didodecyl-2,2′-bithiophene-alt-N, N′-(2-octyldodecyl)-6, 6′-dithiphen-2-yl-isoindigo] (P4TI-3)*

Greenish black solid, 0.26 g (yield = 67%). $^1$H NMR (400 MHz, $CDCl_3$, d): 9.30–9.11 (m, 2H), 7.56–7.50 (m, 4H), 7.22–6.88 (m, 6H), 3.88–3.58 (m, 4H), 2.64–2.46 (m, 4H), 2.26–1.82 (m, 24H), 1.66–1.46 (m, 16H), 1.48–0.96 (m, 70H), 0.96–0.76 (m, 18H).

*3.2.3. Poly[4,4′-didodecyl-2,2′-bithiophene-alt- N, N′-(2-octyldodecyl)-6, 6′-dithiphen-2-yl-isoindigo] (P4TI-4)*

Greenish black solid, 0.23 g (yield = 60%). $^1$H NMR (400 MHz, $CDCl_3$, d): 9.25–9.08 (m, 2H), 7.56–7.34 (m, 4H), 7.17–7.10 (m, 2H), 7.08–6.84 (m, 4H), 3.86–3.52 (m, 4H), 2.86–2.62 (m, 4H), 2.62–2.48 (m, 2H), 2.06–1.80 (m, 6H),1.76–1.64 (m, 8H), 1.64–1.50 (m, 10H), 1.50–0.96 (m, 62H), 0.95–0.74 (m, 18H).

*3.2.4. Poly[3,3′-didodecyl-2,2'-bithiophene-alt-N, N′-(2-octyldodecyl)-6, 6′-di-2,2′-bithiphen-5-yl-isoindigo] (P6TI-3)*

Greenish black solid, 0.19 g (yield = 43%). $^1$H NMR (400 MHz, $CDCl_3$, d): 8.12–8.09 (m, 4H), 7.42 (s, 4H), 7.08–7.04 (m, 8H), 4.70–4.68 (m, 4H), 2.17 (s, 4H), 1.58–1.46 (m, 34H), 1.32–1.14 (m, 82H), 0.91–0.76 (s, 18H).

*3.2.5. Poly[4,4′-didodecyl-2,2′-bithiophene-alt-N, N′-(2-octyldodecyl)-6, 6′-di-2,2′-bithiphen-5-yl-isoindigo] (P6TI-4)*

Greenish black solid, 0.18 g (yield = 41%). $^1$H NMR (400 MHz, $CDCl_3$, d): 8.16–8.06 (m, 10H), 7.18–6.90 (m, 6H), 4.72–4.66 (m, 4H), 2.19–2.14 (m, 4H), 1.58–1.46 (m, 32H), 1.46–0.98 (m, 92H), 0.96–0.76 (s, 18H).

### 3.3. Measurements

The $^1$H NMR (400 MHz) spectra were recorded using a Brüker AMX400 spectrometer in $CDCl_3$, and the chemical shifts were recorded in units of ppm with TMS as the internal standard. The absorption spectra were recorded using an Agilent 8453 UV–visible spectroscopy system. The solutions that were used for the UV–visible spectroscopy measurements were dissolved in chloroform at a concentration of 10 μg/ml. The films were drop-coated from the chloroform solution onto a quartz substrate. All of the GPC analyses were carried out using THF as the eluent and a polystyrene standard as the reference. The TGA measurements were performed using a TG 209 F3 thermogravimetric analyzer. The cyclic voltammetric waves were produced using a Zahner IM6eX electrochemical workstation with a 0.1 M acetonitrile (substituted with nitrogen for 20 min) solution containing tetrabutylammonium hexafluorophosphate ($Bu_4NPF_6$) as the electrolyte at a constant scan rate of 50 mV/s. ITO, a Pt wire, and silver/silver chloride [Ag in 0.1 M KCl] were used as the working, counter, and reference electrodes, respectively. The electrochemical potential was calibrated against $Fc/Fc^+$. The HOMO levels of the polymers were determined using the oxidation onset value. Onset potentials are values obtained from the intersection of the two tangents drawn at the rising current and the baseline changing current of the CV curves. The LUMO levels were calculated from the differences between the HOMO energy levels and the optical band-gaps, which were determined using the UV–vis absorption onset values in the films. The current density–voltage (J–V) curves of the photovoltaic devices were measured using a computer-controlled Keithley 2400 source measurement unit (SMU) that was equipped with a Class A Oriel solar simulator under an illumination of AM 1.5G (100 mW/cm$^2$). Topographic images of the active layers were obtained through atomic force microscopy (AFM) in tapping mode under ambient conditions using an XE-100 instrument.

### 3.4. Photovoltaic cell fabrication and treatment

All the bulk-heterojunction PV cells were prepared using the following device fabrication procedure. The glass/indium tin oxide (ITO) substrates [Sanyo, Japan(10 Ω/γ)] were sequentially patterned lithographically, cleaned with detergent, ultrasonicated in deionized water, acetone, and isopropyl alcohol, dried on a hot plate at 120 °C for 10 min, and treated with oxygen plasma for 10 min to improve the contact angle just before film coating. Poly(3,4-ethylene-dioxythiophene):poly(styrene-sulfonate) (PEDOT:PSS, Baytron P 4083 Bayer AG) was passed through a 0.45-mm filter before being deposited on ITO at a thickness of ca. 32 nm by spin-coating at 4000 rpm in air, and then dried at 120 °C for 20 min inside a glove box. A blend of 1-(3-methoxycarbonyl)propyl-1-phenyl-[6,6]-C71 ($PC_{70}BM$) and the polymer [1:0.5–1:2 (w/w)] at a concentration of 7.5 mgmL$^{-1}$ in chlorobenzene was stirred overnight, filtered through a 0.2-μm poly(tetrafluoroethylene) (PTFE) filter, and then spin-coated (500–3000 rpm, 30 s) on top of the PEDOT:PSS layer. The device was completed by depositing thin layers of $BaF_2$ (1 nm) and Ba (2 nm) as an electron injection cathode, followed by the deposition of a 200-nm-thick aluminum layer at pressures less than $10^{-6}$ torr. The active area of the device was 4 mm$^2$. Finally, the cell was encapsulated using UV-curing glue (Nagase, Japan).

The hole-only devices were fabricated with a diode configuration of ITO(170 nm)/PEDOT:PSS(40 nm)/Polymer:$PC_{70}BM$(50 nm)/$MoO_3$(30 nm)/Al(100 nm). The hole mobility of the active layers was calculated from the SCLC using the J–V curves of the hole-only devices in the dark as follows:

$$J = \frac{9}{8}\varepsilon\varepsilon_0\mu_{h(e)}\frac{V^2}{L^3}\exp(0.89\gamma\sqrt{\frac{V}{L}}$$

where $\varepsilon_0$ is the permittivity of free space ($8.85 \times 10^{-14}$ F/cm); ε is the dielectric constant (assumed to be 3, which is a typical value for conjugated polymers) of the polymer; μ is the zero-field mobility of holes (electrons); L is the film thickness; and $V = V_{appl} - V_r + V_{bi}$), where $V_{appl}$ is the applied voltage to the device, $V_r$ is the voltage drop due to series resistance across the electrodes, and $V_{bi}$ is the built-in voltage.

## 4. Conclusions

In this study, five types of polymers, P4TI, P4TI-3, P4TI-4, P6TI-3, and P6TI-4, were successfully synthesized via the Stille coupling reaction using N,N′-(2-octyldodecyl)-6,6′-di(5-bromothiophen-2-yl)-isoindigo (A1) and N,N′-(2-octyldodecyl)-6, and 6′-di(5-bromo-2,2′-bithiophen-2-yl)-isoindigo (A2) as acceptors while the thiophene donor types were varied. Introduction of a side chain on the donor unit increased the band gap, which led to an increase in the electron-donating properties and a decrease in the ICT effect of the polymers. However, this increase in the band gap could also be reduced by increasing the number of thiophene spacers. Additionally, shoulder peaks were observed in the UV–vis absorption spectra of P4TI and P6TI-4 in both solution and film. However, when side chains were introduced into the P4TI donors (P4TI-3 and P4TI-4), no absorption shoulder peaks were detected in the UV–visible spectra. In contrast to P4TI-3, P6TI-3 with the bithiophene spacers showed absorption shoulder peaks in the film. Thus,

the absence or presence of side chains influenced the appearance of absorption shoulder peaks, and the number of spacers is more significant than the effect of the side chain. XRD measurements revealed that P4TI and P6TI-4 adopted face-on structures, whereas P4TI-3, P4TI-4, and P6TI-3 adopted the edge-on structure common to thiophene-isoindigo-based polymers. The P4TI and P6TI-4 polymers with the face-on orientation that is suitable for OPV cell devices gave rise to higher PCEs because of their superior hole mobility and $J_{SC}$ values compared to the other three polymer types. In particular, when P6TI-4 that formed a face-on structure was used as the active layer, the inverted device performance was fairly high (PCE = 3.5%) with the use of a P6TI-4:$PC_{70}BM$ ratio of 1:2, w/w.

## Notes

All authors have given approval to the final version of the manuscript.

## Acknowledgments

This research was supported by the National Research Foundation of Korea Grant funded by the Korean Government (MEST) (NRF-2009-C1AAA001-2009-0093526) and by the New & Renewable Energy Core Technology Program of the Korea Institute of Energy Technology Evaluation and Planning(KETEP) grant funded by the Ministry of Trade, industry & Energy(MI, Korea) (No. 20133030000180).

## Appendix A. Supplementary data

Supplementary data related to this article can be found at http://dx.doi.org/10.1016/j.polymer.2015.08.003.

## References

[1] F.C. Krebs, N. Espinosa, M. Hösel, R.R. Søndergaard, M. Jørgensen, Adv. Mater. 26 (1) (2014) 29–39.
[2] C.J. Brabec, S. Gowrisanker, J.J.M. Halls, D. Laird, S. Jia, S.P. Williams, Adv. Mater. 22 (34) (2010) 3839–3856.
[3] G. Yu, J. Gao, J.C. Hummelen, F. Wudl, A.J. Heeger, Science 270 (5243) (1995) 1789–1791.
[4] P.P. Khlyabich, B. Burkhart, A.E. Rudenko, B.C. Thompson, Polymer 54 (20) (2013) 5267–5298.
[5] H. Zhou, L. Yang, W. You, Macromolecules 45 (2) (2012) 607–632.
[6] P.M. Beaujuge, C.M. Amb, J.R. Reynolds, Accounts Chem. Res. 43 (11) (2010) 1396–1407.
[7] R. Stalder, J. Mei, J.R. Reynolds, Macromolecules 43 (20) (2010) 8348–8352.
[8] J. Mei, K.R. Graham, R. Stalder, J.R. Reynolds, Org. Lett. 12 (4) (2010) 660–663.
[9] Z. Ma, E. Wang, K. Vandewal, M.R. Andersson, F. Zhang, Appl. Phys. Lett. 99 (14) (2011).
[10] C.-C. Ho, C.-A. Chen, C.-Y. Chang, S.B. Darling, W.-F. Su, J. Mater. Chem. A 2 (21) (2014) 8026–8032.
[11] B. Liu, Y. Zou, B. Peng, B. Zhao, K. Huang, Y. He, C. Pan, Polym. Chem. 2 (5) (2011) 1156–1162.
[12] R. Stalder, C. Grand, J. Subbiah, F. So, J.R. Reynolds, Polym. Chem. 3 (1) (2012) 89–92.
[13] V. Coropceanu, J. Cornil, D.A. da Silva Filho, Y. Olivier, R. Silbey, J.-L. Brédas, Chem. Rev. 107 (4) (2007) 926–952.
[14] M.R. Hammond, R.J. Kline, A.A. Herzing, L.J. Richter, D.S. Germack, H.-W. Ro, C.L. Soles, D.A. Fischer, T. Xu, L. Yu, M.F. Toney, D.M. DeLongchamp, ACS Nano 5 (10) (2011) 8248–8257.
[15] E. Zhou, M. Nakano, S. Izawa, J. Cong, I. Osaka, K. Takimiya, K. Tajima, ACS Macro Lett. 3 (9) (2014) 872–875.
[16] I. Osaka, M. Saito, T. Koganezawa, K. Takimiya, Adv. Mater. 26 (2) (2014) 331–338.
[17] I. Osaka, T. Abe, H. Mori, M. Saito, N. Takemura, T. Koganezawa, K. Takimiya, J. Mater. Chem. C 2 (13) (2014) 2307–2312.
[18] K.W. Song, H.J. Song, T.H. Lee, S.W. Heo, D.K. Moon, Polym. Chem. 4 (11) (2013) 3225–3235.
[19] H.-J. Song, D.-H. Kim, E.-J. Lee, D.-K. Moon, J. Mater. Chem. A 1 (19) (2013) 6010–6020.
[20] H.J. Song, D.H. Kim, E.J. Lee, J.R. Haw, D.K. Moon, Sol. Energy Mater. Sol. Cells 123 (0) (2014) 112–121.
[21] H.J. Song, T.H. Lee, M.H. Han, J.Y. Lee, D.K. Moon, Polymer 54 (3) (2013) 1072–1079.
[22] T. Lei, Y. Cao, X. Zhou, Y. Peng, J. Bian, J. Pei, Chem. Mater. 24 (10) (2012) 1762–1770.
[23] M.S. Chen, J.R. Niskala, D.A. Unruh, C.K. Chu, O.P. Lee, J.M.J. Fréchet, Chem. Mater. 25 (20) (2013) 4088–4096.
[24] (a) H. Farooq, D. Courtier-Murias, R. Soong, H. Masoom, W. Maas, M. Fey, R. Kumar, M. Monette, H. Stronks, M.J. Simpson, A.J. Simpson, Magnetic Reson. Chem. 51 (3) (2013) 129–135;
(b) K. Tatsuki, H. Koichi, NMR Spectroscopy of Polymers, Springer-Verlag Berlin Heidelberg, 2004, http://dx.doi.org/10.1007/978-3-662-08982-8.
[25] C. Kanimozhi, P. Balraju, G.D. Sharma, S. Patil, J. Phys. Chem. B 114 (9) (2010) 3095–3103.
[26] M.C. Scharber, D. Mühlbacher, M. Koppe, P. Denk, C. Waldauf, A.J. Heeger, C.J. Brabec, Adv. Mater. 18 (6) (2006) 789–794.
[27] P. Sonar, H.-S. Tan, S. Sun, Y.M. Lam, A. Dodabalapur, Polym. Chem. 4 (6) (2013) 1983–1994.
[28] X. Zhu, J. Fang, K. Lu, J. Zhang, L. Zhu, Y. Zhao, Z. Shuai, Z. Wei, Chem. Mater. 26 (24) (2014) 6947–6954.
[29] M.S. Almeataq, H. Yi, S. Al-Faifi, A.A.B. Alghamdi, A. Iraqi, N.W. Scarratt, T. Wang, D.G. Lidzey, Chem. Commun. 49 (22) (2013) 2252–2254.
[30] M. Seri, M. Bolognesi, Z. Chen, S. Lu, W. Koopman, A. Facchetti, M. Muccini, Macromolecules 46 (16) (2013) 6419–6430.
[31] J.Y. Lee, M.H. Choi, S.W. Heo, D.K. Moon, Synth. Met. 161 (1–2) (2011) 1–6.
[32] Y. Ren, A.M. Hiszpanski, L. Whittaker-Brooks, Y.-L. Loo, ACS Appl. Mater. Interfaces 6 (16) (2014) 14533–14542.
[33] Y. Geng, J. Cong, K. Tajima, Q. Zeng, E. Zhou, Polym. Chem. 5 (23) (2014) 6797–6803.
[34] S. Izawa, K. Hashimoto, K. Tajima, Synth. Met. 162 (24) (2012) 2201–2205.
[35] D.M. de Leeuw, M.M.J. Simenon, A.R. Brown, R.E.F. Einerhand, Synth. Met. 87 (1) (1997) 53–59.
[36] H. Yi, S. Al-Faifi, A. Iraqi, D.C. Watters, J. Kingsley, D.G. Lidzey, J. Mater. Chem. 21 (35) (2011) 13649–13656.
[37] M.S. Almeataq, H. Yi, S. Al-Faifi, A.A. Alghamdi, A. Iraqi, N.W. Scarratt, T. Wang, D.G. Lidzey, Chem. Commun. 49 (22) (2013) 2252–2254.
[38] Z. Ma, E. Wang, M.E. Jarvid, P. Henriksson, O. Inganas, F. Zhang, M.R. Andersson, J. Mater. Chem. 22 (5) (2012) 2306–2314.
[39] J.-Y. Lee, W.-S. Shin, J.-R. Haw, D.-K. Moon, J. Mater. Chem. 19 (28) (2009) 4938–4945.
[40] H. Zhou, L. Yang, S. Xiao, S. Liu, W. You, Macromolecules 43 (2) (2009) 811–820.
[41] G. Chen, H. Sasabe, Z. Wang, X. Wang, Z. Hong, J. Kido, Y. Yang, Phys. Chem. Chem. Phys. 14 (42) (2012) 14661–14666.
[42] T. Xu, L. Yu, Mater. Today 17 (1) (2014) 11–15.
[43] T. Yasuda, Y. Shinohara, Y. Kusagaki, T. Matsuda, L. Han, T. Ishi-i, Polymer 58 (0) (2015) 139–145.
[44] S. Kim, J.H. Koh, X. Yang, W.S. Chi, C. Park, J.W. Leem, B. Kim, S. Seo, Y. Kim, J.S. Yu, J.H. Kim, E. Kim, Adv. Energy Mater. 4 (6) (2014) (n/a-n/a).
[45] H.-C. Liao, C.-S. Tsao, Y.-T. Shao, S.-Y. Chang, Y.-C. Huang, C.-M. Chuang, T.-H. Lin, C.-Y. Chen, C.-J. Su, U.S. Jeng, Y.-F. Chen, W.-F. Su, Energy & Environ. Sci. 6 (6) (2013) 1938–1948.
[46] K.W. Song, M.H. Choi, H.J. Song, S.W. Heo, J.Y. Lee, D.K. Moon, Sol. Energy Mater. Sol. Cells 120 (2014) 303–309. Part A(0).
[47] Q. Shi, H. Fan, Y. Liu, J. Chen, Z. Shuai, W. Hu, Y. Li, X. Zhan, J. Polym. Sci. Part A Polym. Chem. 49 (22) (2011) 4875–4885.
[48] H. Usta, C. Risko, Z. Wang, H. Huang, M.K. Deliomeroglu, A. Zhukhovitskiy, A. Facchetti, T.J. Marks, J. Am. Chem. Soc. 131 (15) (2009) 5586–5608.
[49] H. Bronstein, Z. Chen, R.S. Ashraf, W. Zhang, J. Du, J.R. Durrant, P. Shakya Tuladhar, K. Song, S.E. Watkins, Y. Geerts, M.M. Wienk, R.A.J. Janssen, T. Anthopoulos, H. Sirringhaus, M. Heeney, I. McCulloch, J. Am. Chem. Soc. 133 (10) (2011) 3272–3275.
[50] K. Parab, K. Venkatasubbaiah, F. Jäkle, J. Am. Chem. Soc. 128 (39) (2006) 12879–12885.